

Investigation of Membrane Actuation for Roll Control of a Micro Air Vehicle

Bret Stanford,* Mujahid Abdulrahim,* Rick Lind,† and Peter Ifju‡
University of Florida, Gainesville, Florida 32611

DOI: 10.2514/1.25356

A class of micro air vehicles uses a flexible membrane wing for weight savings and passive shape adaptation. Such a wing is not amenable to conventional aileron mechanisms for roll control, due to a lack of internal wing structure. Therefore, morphing (in the form of asymmetric twisting) is implemented through the use of a torque-actuated wing structure with thousands of discrete design permutations. A static aeroelastic model of the micro air vehicle is developed and validated to optimize the performance of the torque-actuated wing structure. Objective functions include the steady-state roll rate and the lift-to-drag ratio incurred during such a maneuver. An optimized design is obtained through the use of a genetic algorithm presenting significant improvements in both performance metrics compared with the baseline design.

Nomenclature

α	=	angle of attack
b	=	wing span
C_D	=	coefficient of drag
C_L	=	coefficient of lift
c	=	root chord
F	=	objective function
L/D	=	lift-to-drag ratio
p	=	roll rate
U_∞	=	freestream velocity
W	=	transverse wing displacement
x_{LE}	=	leading-edge coordinate
y_{LE}	=	leading-edge coordinate
z_{LE}	=	leading-edge coordinate
ΔC_p	=	differential pressure coefficient
δ	=	objective function weighting parameter

Introduction

TO EFFECTIVELY navigate through multifarious environments such as urban canyons, a micro air vehicle (MAV), either flown autonomously or remotely piloted, must be very agile. Such agility is typically provided to an aircraft through, among other things, efficient control surfaces. However, using ailerons for the roll control of a MAV presents difficulties, due to the flexible nature of the wings. These thin, undercambered wings are typically built upon a carbon-fiber composite skeleton. The skeleton is then covered with a thin flexible membrane consisting of plastic, polyester, latex rubber, etc. This membrane skin is reinforced with thin strips of carbon-fiber battens. The resulting composite structure is lightweight, yet strong enough to support the wing loading. The flexibility also supplies a certain measure of gust rejection (adaptive washout along the trailing edge helps maintain smooth flight), delays

the onset of stall, and provides smooth poststall behavior [1]. For a MAV, the speed of the gust may be on the same order as the overall flight speed. Maintaining smooth flight can be a challenge for either a remote control (RC) pilot or an autopilot.

Because the flexible membrane MAV wing has little discernible internal structure, the presence of ailerons for roll control is only made possible by sacrificing some of the wing's flexibility [2]. Active wing shaping is an attractive method for supplying roll control to a MAV with thin membrane wings. Morphing, in the form of asymmetric wing twist, takes advantage of the wing's flexible nature: relatively little power is needed to impart substantial structural deformation. Although many forms of wing morphing have been suggested and undertaken, including strain-actuated adaptive wings [3,4], a simpler approach using servos and torque rods is the focus of this paper. An understanding of this thoroughly and successfully flight-tested wing-shaping mechanism represents a crucial step in exploiting the aerodynamic advantages it has to offer. Furthermore, a detailed study can lead to greater insight into the ramifications of wing shaping for vehicles with poor controllability in low Reynolds number environments.

Motivation and Scope

The motivation for this work is to obtain a numerical model suitable for studying the static aeroelastic nature of a micro air vehicle. The vehicle under consideration uses morphing in the form of asymmetric wing twist as a primary means of roll control and is equipped with a wing constructed from flexible composite materials to assist in adaptive washout (gust rejection). Such a model can then be used for future design iterations of the vehicle by considering a numerical procedure wherein various aspects of the vehicle's aerodynamic performance (roll rate, lift, and drag) are optimized by altering the morphing mechanism: thousands of design permutations are admissible.

Typically, the vehicle's rolling performance increases with asymmetrical shape change (barring the case of excessive rotation at the wingtips, which may cause tip stall and adverse rolling moments). Placing torque-rod actuators at the weakest location along the wing promotes large deformation and hence maximizes rolling agility. As with many flexible MAV wings (for which transverse wing deformations may be 10 to 15% of the root chord) there exists a tradeoff between the direct benefit of the shape change (roll rate, in this case) and the efficiency. Compared with a rigid MAV wing, the asymmetrically twisted wing shape will incur a substantial drag penalty. This increase in drag will cause the aircraft to decelerate and lose altitude. The reduction in dynamic pressure will decrease the effectiveness of the torque actuation and jeopardize the ability of the vehicle to maintain a desired roll rate. Furthermore, the asymmetric

Presented as Paper 2162 at the 47th AIAA/ASME/ASCE/AHS/ASC Structures, Structural Dynamics, and Materials Conference, Newport, RI, 1–4 May 2006; received 22 May 2006; revision received 12 February 2007; accepted for publication 15 February 2007. Copyright © 2007 by Bret Stanford. Published by the American Institute of Aeronautics and Astronautics, Inc., with permission. Copies of this paper may be made for personal or internal use, on condition that the copier pay the \$10.00 per-copy fee to the Copyright Clearance Center, Inc., 222 Rosewood Drive, Danvers, MA 01923; include the code 0021-8669/07 \$10.00 in correspondence with the CCC.

*Research Assistant, Department of Mechanical and Aerospace Engineering.

†Assistant Professor, Department of Mechanical and Aerospace Engineering.

‡Professor, Department of Mechanical and Aerospace Engineering.

drag distribution over the actuated wing will cause a yaw moment. At the low speeds typical of MAV flight, this coupling between the roll and yaw moments will compromise the stability of the wing and may cause the MAV to crash. As such, the roll analysis of low-speed flexible membrane wings must include considerations for drag efficiency; this work proposes to elucidate the tradeoff curves between the two.

A complete description of the micro air vehicle in question will be given in terms of typical flight characteristics, as well as a thorough understanding of the vehicle's baseline torque-actuated wing structure. A justification of the mechanism's baseline design will be discussed, in addition to a rationale behind the belief that a better design should exist. A steady aeroelastic model of the wing is formulated, composed of a structural model (finite elements of the composite wing and the morphing mechanism), a commercially available vortex-lattice code, and an algorithm that communicates between the two. A basic multi-objective optimization scheme is detailed, including the use of a convex combination of multiple-objective functions (roll rate, lift, and drag), the Pareto optimal front, and genetic algorithms.

Micro Air Vehicle

The ever-decreasing size of micro air vehicles represents successful efforts along a multidisciplinary front, with technological advances in materials, fabrication, electronics, propulsion, actuators, sensors, and control. A MAV should be inexpensive and expendable, suitable for situations in which a larger vehicle is not. Such circumstances may arise in both military (battlefield surveillance and bomb damage investigations) and civilian sectors (agriculture/crop management and wildlife surveillance).

As discussed earlier, the hallmark of many MAVs is an inherent flexibility built into the wing, specifically, a membrane wing. This method of designing wings was shown to assist in delaying the onset of stall [5] and can generate a sufficient amount of lift without an overbearing weight. An extensive library of work has developed in the last few years concerning the analysis of flexible MAV wings, both in an experimental and numerical sense. A detailed study concerning the influence of deformability on a MAV's classical aerodynamic parameters was conducted via experimental wind-tunnel analysis for a variety of flight conditions [5]. Projection moiré interferometry [6] was used to measure the out-of-plane displacements over a wing, whereas cross-correlation using stereo triangulation [7] successfully recovered the complete displacement field over a membrane wing MAV and thereby also garnered information concerning the membrane strain. Numerically, Lian et al. [8] effectively modeled the unsteady aerodynamics over a membrane MAV wing, thereby demonstrating the relationship between membrane dynamics and flight performance.

Aircraft Description and Construction

The MAV under consideration in the current work can be seen in Fig. 1. The wingspan is 28 in., the aspect ratio is 6, and the wing area is 129 in.². The airframe is constructed entirely from two layers of bidirectional plain-weave carbon fiber, both in the ± 45 -deg direction. The fuselage is designed to hold the necessary flight components including servos, autopilot, video camera, and batteries. An empennage is fixed to the fuselage, with elevator and rudder control surfaces hinged to the horizontal and vertical stabilizers, respectively.

The wing, which is fixed to the top of the fuselage, is also designed to hold various flight components: the propulsion system, the global positioning system, and the actuation servo (to be discussed next) are all attached to the underside of the wing, above the fuselage. The leading edge and the center of the wing are constructed from three layers of bidirectional plain-weave carbon fiber, with the outer layers in the ± 45 -deg direction and the inner layer in a 0/90-deg configuration. Battens, constructed from thin strips of unidirectional carbon fiber (two layers, with the fiber direction parallel to the batten), extend from attachment points along the membrane/weave boundary.



Fig. 1 Micro air vehicle.

To the carbon-fiber skeleton is affixed a thin membrane skin, for which two materials are commonly used. In the case of the MAV seen in Fig. 1, the skin is an inextensible polyester fabric called Icarex©. The polyester is included in the carbon-fiber lay-up process, and the resin serves to seal the skin to the wing. However, latex provides a wing with greater flexibility (largely due to its in-plane extensibility, whereas the polyester merely serves to communicate displacement between adjacent battens) and also offers the designer a certain amount of control over the wing's stiffness: the pretension in the membrane skin can be varied along different directions. The latex rubber, because it cannot withstand the heat of the composite's cure cycle, is fixed to the wing afterwards. The membrane sheet is stretched about a frame and then sealed to the wing by a spray glue adhesive. A polyester skin is usually preferred in MAV design and flight testing for practical and commercial reasons: the onset of latex degradation due to sunlight, fingertip oil, and repeated crashes is very rapid. Because these factors are not an issue in this largely numerical study, an extensible latex rubber skin will be the focus of this work.

Wing Actuation

The value of morphing as a control effector is well realized at the micro-air-vehicle scale: a relatively small amount of power is needed to inflict a substantial shape change to a wing operating at low dynamic pressures [2]. This is especially true for a flexible membrane wing. The actuation considered in this paper comes in the form of wing twisting to achieve roll control. The underlying mechanism of this shape change can be seen in Fig. 2. Torque rods run spanwise down the length of each wing and are allowed to freely twist within metal sleeves glued to the wing toward the leading edge. After a 90-deg bend, the rods are fastened to a batten with Kevlar© threads. Both left and right rods are connected to a single servo housed on the underside of the wing. The connective linkage is constructed in such a way that a single command to the morphing servo imparts equal and opposite deformation fields to either side of the wing. The wing twisting increases or decreases the angle of attack, causing

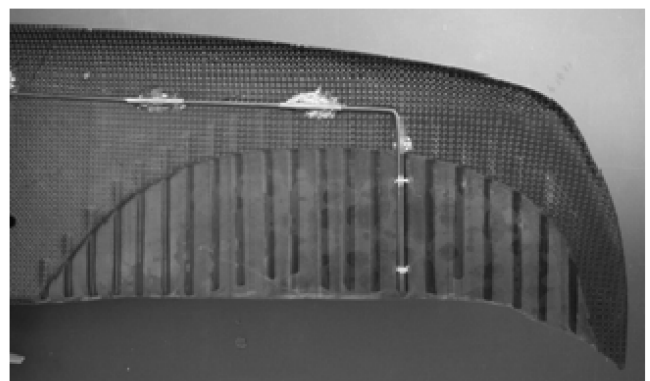


Fig. 2 Torque rod embedded within the membrane wing.

differential aerodynamic forces and a subsequent roll moment. The leading edge is constructed from relatively stiff carbon-fiber plies, and so the majority of deformation is expected to be concentrated along the trailing edge, in which the latex membrane is the predominate material. As such, the wing shaping caused by the torque rods behaves in a manner similar to conventional ailerons.

Numerical MAV Modeling

Static Structural Modeling

Three different types of finite elements are used to model the MAV wing seen in Fig. 2: membrane elements (for the latex skin), beam elements (for the battens and the torque rods), and plate elements (for the carbon-fiber laminate). The remainder of the vehicle (fuselage and horizontal and vertical stabilizers) is considered to be rigid. A schematic of the unstructured finite element mesh can be seen in Fig. 3. This mesh is mirrored about the root chord to model both the left and the right wing: a necessary step due to the unsymmetrical pressure and displacement fields incurred during a roll maneuver.

The thin membrane skin is modeled with a three-node membrane element. Typical membrane mechanics hallmarks such as material and geometrical nonlinearities [8,9] are assumed negligible for small deflections. Such an element's constitutive equation is formulated by adding stress-stiffening terms to the standard plate equations and then equating the bending stiffness to zero (the latex membrane is thin enough that it provides no resistance to bending). This leaves the well known Poisson's equation, with out-of-plane displacement as the dependent variable [10]. This formulation assumes that the strain in the membrane is constant (equal at all times to the prestrain).

The thin strips of unidirectional carbon fiber that serve as battens are well modeled by standard two-node Euler-Bernoulli beam elements, with one out-of-plane displacement and one bending rotation degree of freedom per node. A similar element is suitable for the torque rods (but with torsional rotation degrees of freedom superimposed, as well). As seen in Fig. 3, only the last two legs of the torque rod are modeled, rather than the complete linkage system. The twisting actuation from the servo is modeled by applying a torque to the free end of the rod. This end of the rod is constrained from moving or bending, whereas the final leg of the rod is attached to the batten. The remainder of the rod is free. Discrete Kirchhoff plate elements are used to model the wing's bidirectional carbon-fiber skeleton. Each node contains three degrees of freedom (one out-of-plane displacement and two rotations) and so, like the previous two elements, does not model in-plane stretching, transverse shear strain, or drilling motions. The orthotropic nature of the composite laminate is accounted for by using a mosaic model. This models the plain-weave composite as two unidirectional plies (with orthogonal orientations) occupying the same plane. A series of system-identification and model-validation studies aimed at determining the appropriateness of the preceding finite elements for predicting the deformation of membrane MAV wings with composite skeletons was conducted [11]. Weights are hung from a series of locations over the wing and stereo triangulation (visual image correlation) is used to measure the resulting wing deformation. These data are then used to

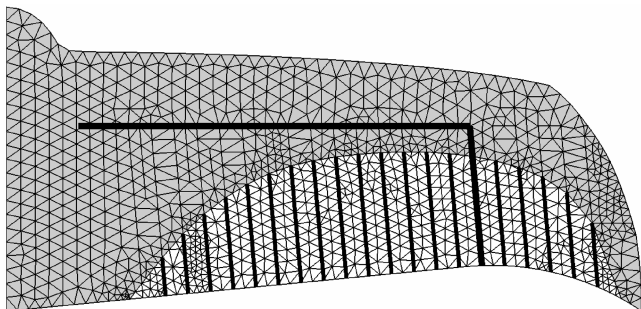


Fig. 3 Finite element mesh: plate elements (gray triangles), membrane elements (white triangles), beam elements for the battens (black lines), and beam elements for the torque rod (thick black line).

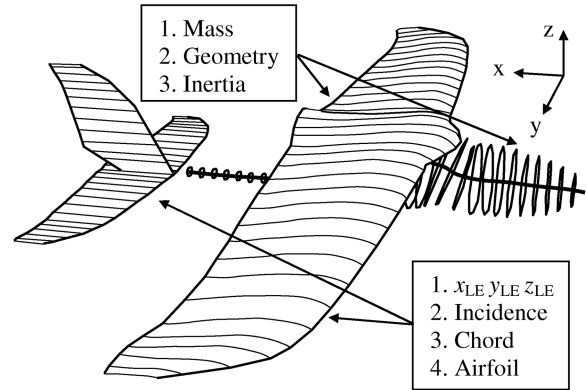


Fig. 4 AVL program inputs.

tune the material parameters of each finite element. Further information is given by Stanford et al. .

Aerodynamic Modeling

The forces that accumulate over a flexible MAV wing are simulated using Athena Vortex Lattice (AVL), an inviscid vortex-lattice-method code developed by researchers at the Massachusetts Institute of Technology [13]. The code takes vehicle geometry, inertial properties, and flight conditions as input, and outputs the ΔC_p distribution over the wing surface (the difference in pressure coefficient between the lower and upper wing surfaces) as well as various aerodynamic quantities of interest. A graphical description of the AVL inputs is seen in Fig. 4. Lifting surfaces are constructed by providing airfoil information at several span stations. The resulting structured mesh of wing panels is given in Fig. 5; each panel contains a horseshoe vortex. AVL then generates and solves the system of equations governing the strength of each vortex filament; the tangency condition is enforced at each control point (located at the quarter chord of each panel), wherein each panel must coincide with the streamlines of the flow.

For rolling-maneuver simulations, AVL iterates until the rolling moment is zero (for a steady roll rate) by computing the roll damping. AVL linearizes the aerodynamics, and so the roll damping is the combination of the $C_{L\alpha}$ slope for each wing section (series of horseshoe vortex filaments at each span station) and the associated moment arm. As the aircraft approaches a steady-state roll, the roll damping remains constant (due to the linear aerodynamics), but the system has neared an equilibrium and will stop accelerating in roll. Once this steady rolling condition was determined, the tangency condition is again applied for each panel, and the induced drag from each vortex is summed to calculate the drag associated with the rolling maneuver. The zero-lift drag (C_{D0} , presumably due to viscous and separation effects not accounted for in the inviscid aerodynamic solver) must be estimated by the user based upon either the frontal-projection area or the wetted area.

Certainly there is questionable validity in using an inviscid code to model the aerodynamics of a vehicle for which the relatively low Reynolds number ($\sim 200,000$) indicates the possible importance of

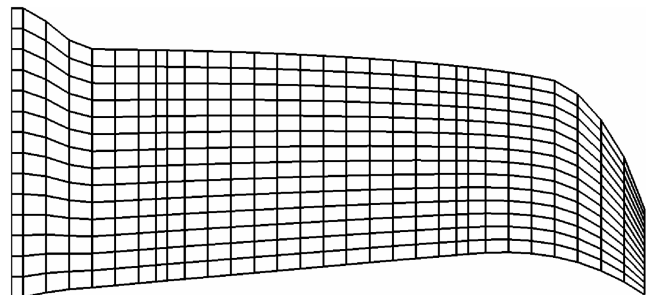


Fig. 5 Structured mesh of wing panels generated by AVL.

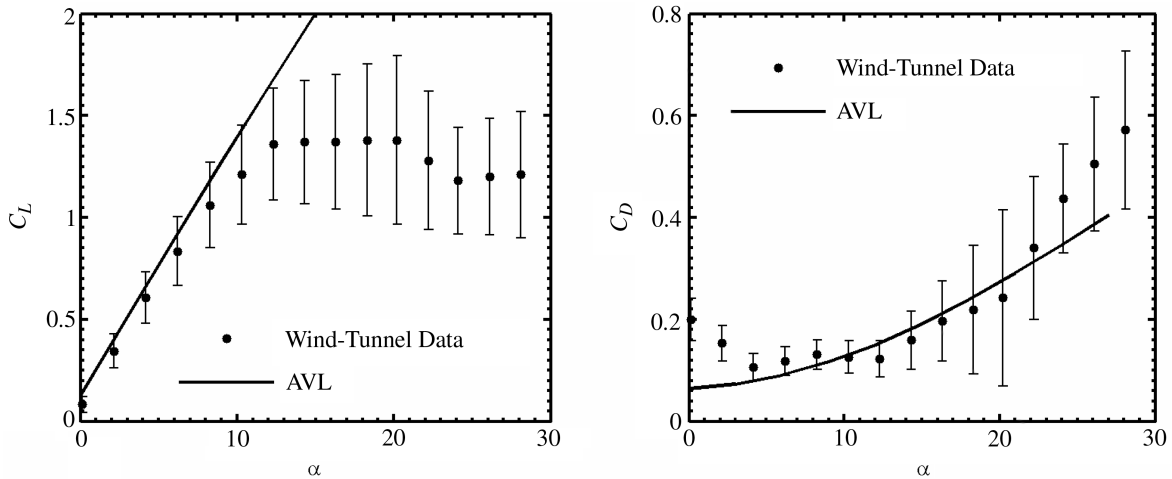


Fig. 6 Computed and measured aerodynamics in steady level flight; $U_\infty = 15$ m/s.

viscous drag, flow separation, etc. Computed (from AVL) and measured (from a wind-tunnel analysis [5]) aerodynamic coefficients of the flexible wing in steady level flight are given in Fig. 6. The results indicate that AVL is able to predict the lift to within experimental error bars up to the stall angle. Drag, as expected, is significantly underpredicted at low angles of attack, though the correlation is suitable at moderate angles (greater than 3 deg). Validation of computed roll rates cannot be measured in the wind-tunnel setup used here; flight testing is required. Data gathered via onboard gyros and accelerometers [2] indicate a suitable correlation of the roll-time constant (eigenmode) with the computations used in this paper. Further information is given by Abdulrahim et al. [2]. Any modeling errors inherent with the use of AVL (or the aforementioned structural model) should not deter its value as an analysis tool. The model will merely provide a comparison of the attributes of design A to design B and should be able to reliably predict an improvement in the baseline design.

Fluid-Structure Interaction

The following steps are taken to complete the static aeroelastic model of the flexible MAV. AVL first computes the ΔC_p distribution over an undeformed wing. These values are then interpolated from the mesh of Fig. 5 to that of Fig. 3 and converted to nodal forces. Equal and opposite torques (to simulate the servo) are applied to the free end of each torque rod (seen in Fig. 3), and the displacement field over the wing is computed. No feedback control to the servo is modeled; the output torque to the wing is specified before the computation and is independent of the wing's resistance to twisting. This represents a minor deviation from the actual situation: the servo is position-controlled within a torque range. The torque rod will stop twisting when the structural torsional stiffness of the wing is equal to the servo torque; the equilibrium position will be slightly different for disparate actuation structures. Fixing the variable, however, will highlight the associated aeroelastic optimization process: improvements in system performance for a given input. A constant value of $0.04 \text{ N} \cdot \text{m}$ is used for all of the computations in this work.

The displacement field is converted into an AVL input file by computing the new leading-edge locations, chord, incidence, and airfoils at 55 span locations from left to right wingtip. This information is again inputted into AVL (when confronted with an unsymmetrical wing geometry, AVL iterates its solution until the coefficient of rolling moment is zero, and returns a steady roll rate, a process that usually takes three iterations). Information is passed between the finite element code and AVL until the solution converges to within an acceptable error. Less than 2% change in wingtip displacement can usually be obtained within 10 iterations. The entire procedure is conducted within the MATLAB environment, by using in-house FEA codes [12] and AVLab, an in-house simulation interface developed for AVL [14].

Wing Actuation with a Single-Torque Rod

The normalized transverse displacement field of a MAV engaged in a roll maneuver can be seen in Fig. 7. Displacements are sampled from the trailing edge of the wing. The torque-rod placement is identical to that seen in Fig. 2 (the portion of the rod that comes in contact with the membrane wing is located at 68% of the semispan), a torque-actuation mechanism that will continually be referred to as the baseline design. Two different cases are presented (both with the same input moment to the torque rods). The first assumes that the wing is impervious to aerodynamic loading: the wing assumes a morphed shape as a result of the torque rods, but no further deformation (due to the fluid-structure interaction) is accounted for. As expected, the displacement field is asymmetric about the root chord; the tip of the left torque rod moves up $0.12c$, whereas the right rod moves equal and opposite. The displacement field is localized about the torque rod. The stiff leading edge of the wing (constructed from carbon fiber) remains largely unaffected, outside of a slight bending deformation. Within the membrane skin, due to the extensibility of the latex, only the regions lying within an inch of the rod experience any sizable deformation. The wing twisting provided by the torque-rod structure is a combination of aerodynamic and geometric twist. The former dominates in the membrane regions (local changes in camber), whereas the latter is present toward the carbon-fiber wingtips (for which the airfoil section is largely preserved, but rotated).

Adding the effect of the pressure loads (Fig. 7) destroys the effect of the antisymmetric nature of the displacement field: both sides of the wing bend up. This pushes both torque rods up (compared with the deformation without aerodynamic loads) and certainly decreases the

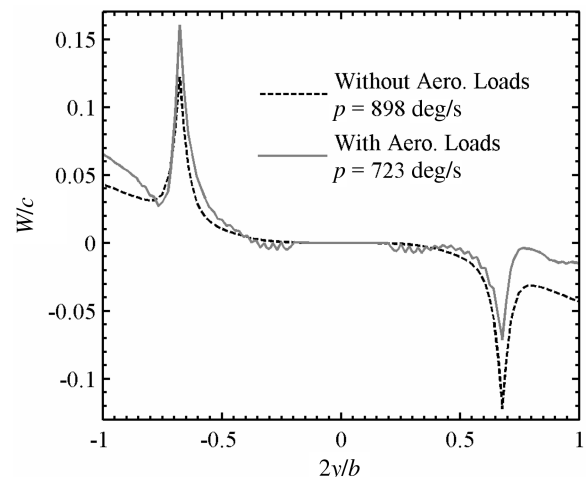


Fig. 7 Normalized transverse displacement of the trailing edge; $U_\infty = 15$ m/s and $\alpha = 3$ deg.

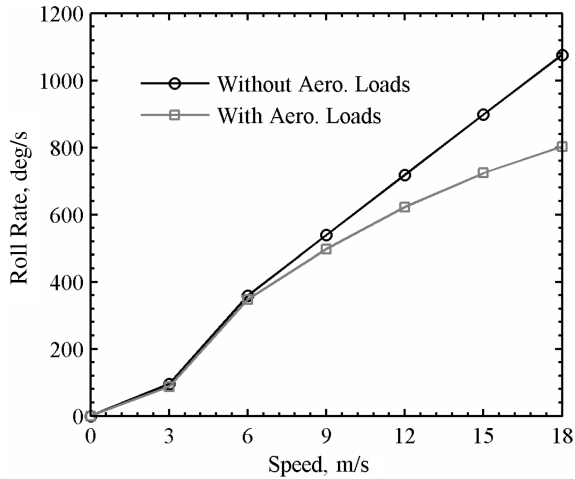


Fig. 8 Loss of roll rate due to aerodynamic deformation; $\alpha = 3$ deg.

effectiveness of that on the right. Furthermore, both torque rods are now subject to an unfavorable twisting moment. For example, the rod on the right actuates the wing to increase the local angle of incidence. The resulting nose-down pitching moment will somewhat untwist the wing, decreasing the effectiveness of the torque rod. The net result is a decrease in steady roll rate by 20% compared with the wing without aerodynamic loading. Other aeroelastic effects are found in the membrane regions of the wing: adaptive inflation of the latex skin between the carbon-fiber battens is clearly evident. Further data highlighting a loss of roll rate in flexible MAVs can be seen in Fig. 8; as expected, roll performance decays with higher dynamic pressures. The detrimental effect of wing flexibility on roll rate is a well known phenomenon. Unlike the use of a hinged trailing-edge surface (for which a force is applied locally to the trailing edge of the wing), global torque-actuation of the wing will never result in roll reversal: the torque is applied directly to the wing in the proper direction. Increased dynamic pressures can result in a completely ineffective torque rod, however, but Fig. 8 indicates that this would occur at a speed well above the expected flight range of MAVs. Convention-

ally, the unfavorable aerodynamic twisting moment is counteracted by stiffening the wing [15]. Because this method cannot be expected to produce favorable results in a MAV wing that uses its inherent flexibility to engage in a roll maneuver, we attempt to improve roll performance by making changes to the torque-rod wing actuation mechanism.

We restrict ourselves, for the time being, to morphing-mechanism designs that contain a single torque rod: the spar that runs from the servo, spanwise down the wing, is only attached to a single rod that connects to the membrane skin. The torque rod must be fastened to the membrane skin at batten locations (otherwise, the skin will rip); a cursory glance of Fig. 2 reveals 20 such designs. The rolling performance of each of these torque-rod designs is summarized in Fig. 9. Intuition would imply that the farther the torque rod is placed from the root of the wing, the higher the roll rate. Any basic structure subject to torsional loading sees higher deformations as the torque moves farther and farther away from the fixture point. Usually, for wing-shaping applications, large deformations lead to large roll rates (however, flight testing has also indicated that excessive wing actuation toward the wingtip can cause tip stall and an adverse roll moment, thus explaining the torque-rod location in the baseline design). As such, the torque-actuated wing designs with torque rods located too close to the root produce negligible roll rates.

Contrary to the argument given earlier, the curve of Fig. 9 peaks at an intermediate torque-rod location, rather than at the wingtip. This is due to the composition of the wing at each torque-rod location: it is mostly carbon-fiber composite toward the root and at the wingtip (short battens) and mostly latex membrane at intermediate locations along the wing (long battens). Obviously, the compliant membrane structure is conducive to large torque-rod movements. The optimum design of Fig. 9 (torque rod located at 75% of the semispan) represents a slight improvement in roll over the baseline design (torque rod located at 68% of the semispan): an increase of 10%.

As discussed earlier, the large displacements used to force the membrane wing into a rolling maneuver will generate a significant amount of asymmetric drag. This may lead to deceleration and stability problems and must be monitored. The lift and drag characteristics of each morphing-mechanism design are given in Fig. 10. As expected, the torque-rod location has the opposite effect

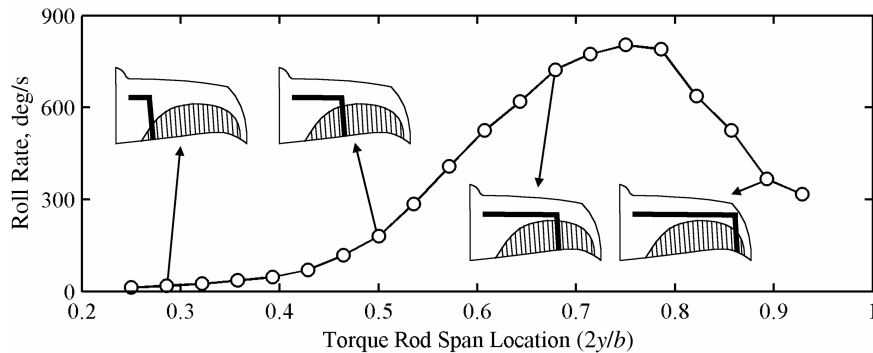


Fig. 9 Maneuverability of a MAV with different torque-rod placements; $U_\infty = 15$ m/s and $\alpha = 3$ deg.

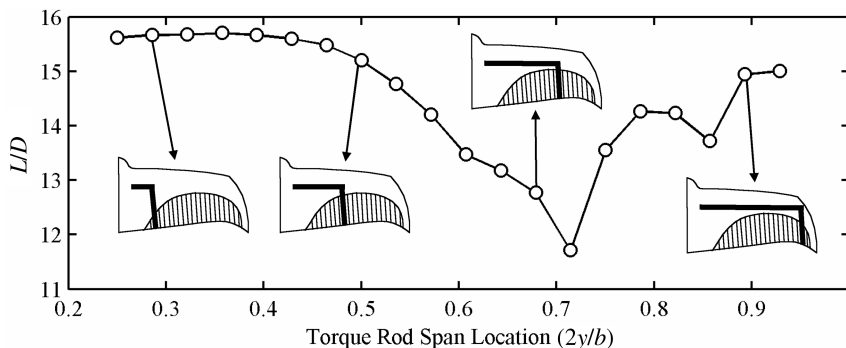


Fig. 10 Efficiency of a MAV with different torque-rod placements; $U_\infty = 15$ m/s and $\alpha = 3$ deg.

of the data in Fig. 9: effective wing shaping produces unfavorable L/D ratios (the lift and drag considered here are those measured during the roll maneuver, rather than during steady level flight). Indeed, the greatest aerodynamic efficiency ($L/D = 15.7$) is provided by a design with almost no roll rate (36 deg/s); the minimal wing shaping provided by the ineffective torque rod preserves the intended streamlined aerodynamic shape. Effective wing actuation for large displacements results in the nonoptimal shapes seen in Fig. 7. The torque-rod actuation has little effect on the carbon-fiber leading edge, and so the wing shape develops a tangent discontinuity in the chordwise direction, increasing the drag. Significant savings in L/D are available to the designer (up to 16.3% improvement over the baseline design), but only by sacrificing most of the vehicle's agility. Conversely, the design with the optimal roll rate in Fig. 9 also provides an increase in efficiency (6.5% over the baseline).

Wing Actuation with Multiple Torque Rods

Having only achieved minor improvements in roll rate and L/D over the baseline design when restricting the actuation mechanism to a single torque rod, further progress is sought through the use of multiple torque rods. In this configuration, a single spar would still run spanwise down the wing, but would now attach to multiple rods that fasten to the membrane wing. Because the torque rod seen in Fig. 2 is monolithic (a single rod is bent at several locations), a multiple-torque-rod configuration would require some welding. A doctored image of a feasible two-rod design is given in Fig. 11 to provide an example of what a multiple-rod configuration might look like. Why can we expect a mechanism with multiple torque rods to outperform any of the data presented in the previous section? Multiple torque rods must now share a single servo torque. Although the local wing twist at each rod will decrease (compared with the wing actuation caused by a single torque rod), the end result should provide a more global (rather than the local pattern seen in Fig. 7) displacement field over the wing, possibly increasing the roll rate. Furthermore, the unfavorable twisting moment is reduced by the smaller-wing actuation; multiple-torque-rod configurations will lose less agility, due to aeroelastic effects. Drag penalties should also be reduced. Multiple-torque-rod configurations will increase the structural weight and roll inertia of the vehicle, but this is not felt to be a critical concern. For example, welding five torque rods (roughly 3-in. long each) to the leading-edge rotating spar will add no more than 10 g to the overall weight. Additionally, the MAVs carry the majority of their payload in the fuselage, and so the significant roll damping will typically overshadow the extra roll-inertia effects. Therefore, the slightly higher roll inertia associated with multiple-torque-rod configurations can achieve better steady-state roll rates without notably affecting the roll acceleration.

By allowing for the possibility of multiple torque rods, the required optimization procedure increases by several orders of complexity. With only one torque rod, only 20 designs are feasible. This leads to the simple enumeration procedure presented in Figs. 9 and 10, in which every possible design can be tested. Considering wing-actuation mechanisms with multiple torque rods allows for over a million possible discrete design permutations (still restricting torque-rod locations to coincide with wing battens). Complicating

the matter is the presence of two aerodynamic quantities of interest: roll rate and L/D , making the design process a multi-objective optimization. This study will identify the two designs that maximize the two objective functions and also the locus of designs that strike a compromise between the two. Providing the designer with a set of compromises is a necessary step in the testing of flexible, maneuverable, low-speed vehicles. Depending on a number of factors, it may not be in the designer's best interest to use a MAV design with maximum rolling agility. Low-fidelity autopilot systems or inexperienced RC pilots (which are typically the case) may not be able to keep pace with a highly maneuverable vehicle. The unfavorable scaling of MAVs is another factor. There is a significant drop in L/D as the Reynolds number drops below 100,000 (the flight regime of the vehicle considered here). Using a torque-actuated wing structure with a roll rate comparable to the baseline design, but an improved L/D , may present itself as an attractive option as the size of MAV wings continues to decrease.

With two objective functions, we can no longer find a single best design, because we can expect roll rate and L/D to conflict (as seen in Fig. 9 and 10): a design that decreases one will increase the other. The set of compromise solutions is called the Pareto optimal front [11]. This set comprises designs that are *nondominated*: no design exists with a better L/D and a better roll rate. Additional information not taken into account during the optimization procedure can then be used to select an optimal design from the Pareto set. The approach used here to construct the front is by optimizing a convex combination of the two normalized objective functions p and L/D [11]. Maximize

$$F = \delta \cdot p + (1 - \delta) \cdot L/D \quad (1)$$

by changing the number of torque rods and the position of each, where δ varies between zero and one, for which several values are chosen successively. A single-objective optimizer then produces the designs that lie on the Pareto optimal front (as long as the set is convex). A genetic algorithm (GA) is used for single-objective optimization. Genetic algorithms are well suited to problems in which design variables are required to take a binary form [16] and are thus appropriate for the problem at hand. Though several multi-objective optimization schemes outperform the weighted-sum approach in terms of efficiency (the MOGA [11] approach, for example), the GA is expected to have a high success rate, and efficiency is not a major concern. Figure 12 shows how a morphing-mechanism design can be translated to a chromosomal binary string (three random mechanisms are shown).

The genetic algorithm begins with an initial population of chromosomes. This is typically done by assigning zeros and ones to the strings in a random fashion, but here we opt to use the 20 designs shown in Fig. 9. Three main operations are then employed at each generation to converge on an optimum design: reproduction, crossover, and mutation. In the former, chromosomes with good fitness are copied to the next generation. A torque-rod design is sent to the aeroelastic solver and the steady-state roll rate and L/D are calculated for a given servo torque output, flight speed, and angle of attack. These values are then sent to Eq. (1) and, for a given value of δ , the fitness of the design is returned to the GA. After reproduction, the

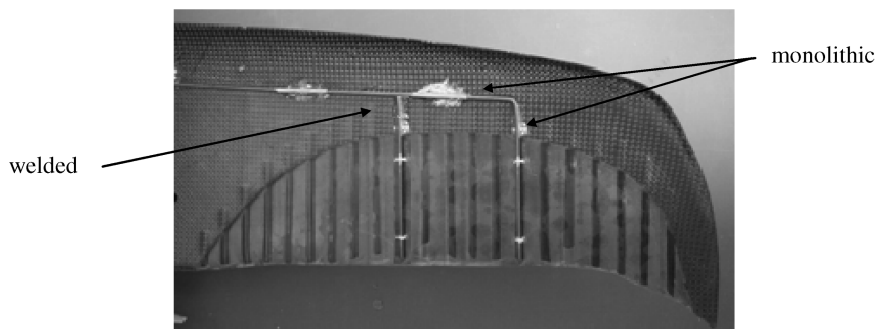


Fig. 11 Multiple torque rods embedded within the membrane wing.

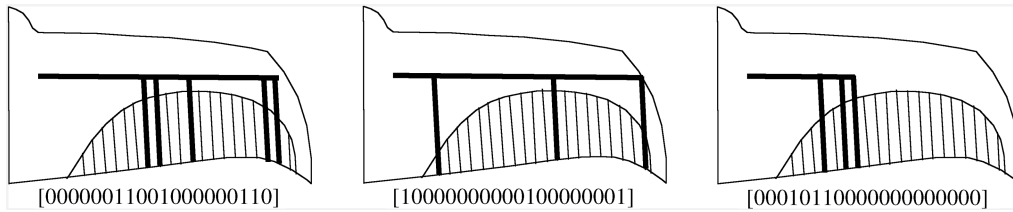


Fig. 12 Representation of a torque-rod mechanism by a binary string.

designs are randomly paired off for crossover or mating. Mutation is also employed to promote diversity within the design population by randomly switching a bit value from zero to one or vice versa. More details concerning the working mechanism of a genetic algorithm are widely available [11,16]. MATLAB's genetic algorithm toolbox [17] is employed for the current work. The population size is 20, the elitism count is 2, and the stopping criterion is 15 generations without an improvement in the best fitness. Reproduction is via a two-point crossover function with a 0.8 crossover fraction, and a uniform mutation function is used with a 0.01 mutation rate.

The results from the multi-objective optimization are given in Fig. 13. The design with the highest roll rate [the right-most point on the Pareto optimal front, found when δ is set to unity in Eq. (1)] represents a 34% improvement in roll rate over the baseline design (Fig. 2) and a 6% improvement in L/D . Unsurprisingly, this design is found by grouping several torque rods about the same location that was found to be optimum in Fig. 9. The design with the highest lift-to-drag ratio [the left-most point on the Pareto optimal front, found when δ is set to zero in Eq. (1)] provides a 23% improvement in L/D , but a decrease in roll rate by almost 97%.

These results are similar to those seen in Fig. 10. The best lift and drag characteristics in a flexible MAV wing can be obtained by making the torque rod as ineffectual as possible. Obviously, from a designer's standpoint, this design with optimal lift and drag is useless. Only the torque-rod mechanisms located within the shaded region of Fig. 13 (designs that dominate the baseline design in both roll and L/D) can be realistically viewed as potential candidates. The general topology of Fig. 13 can be described as follows: the Pareto optimal front generally comprises designs with multiple torque rods grouped closely together. Displacements and wing twists (discussed in detail next) are relatively small, which constitute a low drag penalty associated with deformation. Roll rates for these designs are

maintained at a high level for the reasons given earlier: low unfavorable twisting moments and global wing-twisting behavior. The set of dominated designs that constitute the lower border of the locus of feasible designs in Fig. 13 generally comprises single-torque-rod designs. Wing actuation is large enough to achieve high roll rates, though the wing efficiency suffers. An important aspect of the torque-actuated wing structures with multiple rods is their (generally) superior roll rates compared with single-rod designs. An equally significant feature is their ability to achieve the same maneuverability as the single-rod designs, but with significantly higher efficiency.

The evolutionary history of the population when fitness is evaluated with a δ of unity is given in Fig. 14. The design with the best fitness at the start of the algorithm is the optimum in Fig. 9 (the initial population is a set of single-rod designs), and the converged solution is the right-most point on the Pareto optimal front. Similar plots can be given for the remainder of the front. Of ten genetic algorithm runs (one of which is shown in Fig. 14), the GA is able to locate the wing-shaping design with the optimal roll rate five times. The remainder of the optimization runs are unable to converge past the design with the best fitness within generations 10 through 18 in Fig. 14. Given that the genetic algorithm relies on several stochastic processes, there is no guarantee that the final solution of Fig. 14 is the global optimum for roll rate, but nonetheless presents a significant improvement over the baseline design. As the value of δ is decreased toward zero, improvement in the objective function generally takes fewer iterations than that seen in Fig. 14. The repeatability of locating the optimum designs decreases as well, because many disparate designs have similar L/D ratios.

The wing-displacement fields of the baseline design, the design with optimal roll rate, and the design with optimal lift and drag can be seen in Fig. 15. As before, displacements are sampled from the

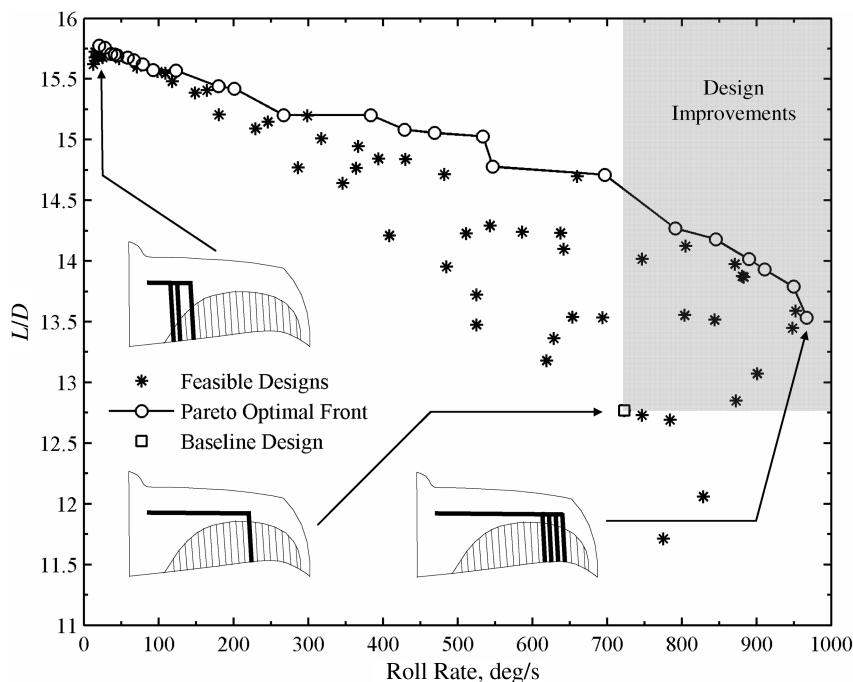


Fig. 13 Pareto tradeoff curve of torque-rod designs; $U_\infty = 15$ m/s and $\alpha = 3$ deg.

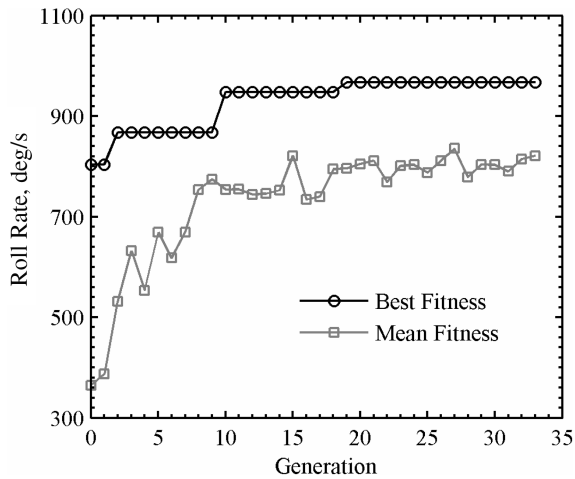


Fig. 14 Evolutionary history of the optimization procedure with $\delta = 1$, $U_\infty = 15$ m/s, and $\alpha = 3$ deg.

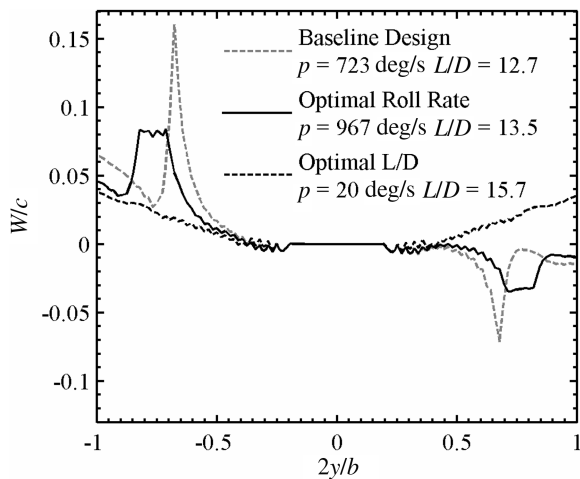


Fig. 15 Normalized transverse displacement of the trailing edge; $U_\infty = 15$ m/s and $\alpha = 3$ deg.

trailing edge. As expected, although the maximum displacement seen from the optimum roll rate design (8% of the root chord) is significantly less than the baseline single-torque-rod design (16% of the root chord), the displacement field is now of a more global nature (resembling a conventional aileron flap) and results in a higher steady-state roll rate. The locus of appreciable wing displacement is

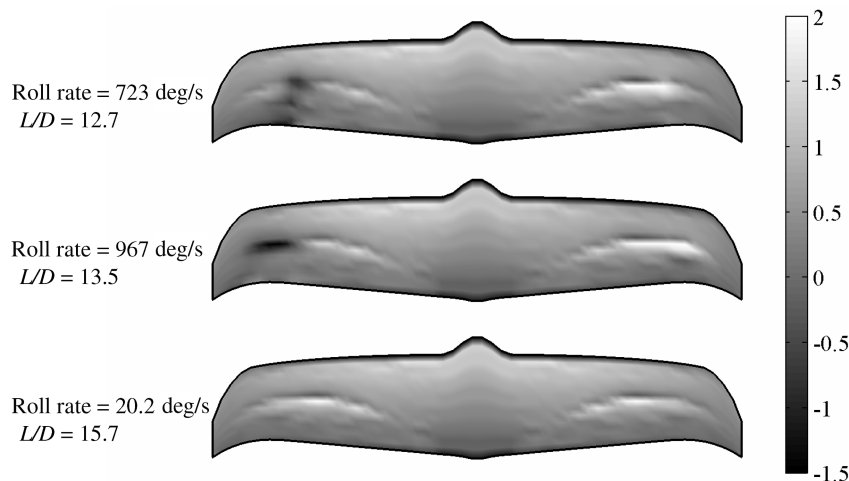


Fig. 16 Computed ΔC_p of the baseline design (top), the design optimized for roll (center), and the design optimized for L/D (bottom); $U_\infty = 15$ m/s and $\alpha = 3$ deg.

moved farther toward the wingtip, increasing the moment arm, and further improving roll performance. The displacement field of the design with optimal lift and drag is nearly symmetrical about the root, as evidenced by this design's extremely low roll rate. This is essentially the MAV's static aeroelastic response in steady level flight, further reinforcing the notion that efficient wing shaping can be achieved with smooth wing shapes and small deformations.

The differential-pressure-coefficient fields (as predicted by AVL) of the baseline design, the design with optimal roll rate, and the design with optimal lift and drag can be seen in Fig. 16. All three distributions show large pressure gradients at the boundary between the latex membrane and the plain-weave carbon fiber. This is due to the adaptive inflation of the membrane at this location (clearly seen in Fig. 15), which increases the camber of the wing. As the air flows over the wing, it must rapidly change direction to travel over this inflated membrane shape. The flow over the upper surface decelerates to make this turn, causing a pressure spike, which corresponds to a negative local transverse aerodynamic force. The flow then accelerates over the location of maximum camber. This typically coincides with the location of pressure recovery over the upper wing surface and causes a peak in transverse aerodynamic force.

None of the three torque rods designs shown in Fig. 16 have appreciably dissimilar pressure fields over the right side of the MAV wing. As discussed earlier, the downward motion caused by the right torque rod is counteracted by the aerodynamic loading, limiting its effectiveness. The opposite is true on the left side of the MAV wing: the baseline design shows a region of negative differential pressure localized about the single torque rod. When the design is optimized for roll performance, both the magnitude and the moment arm of the downward force are increased, though the affected region no longer extends all the way to the trailing edge. As before, the design with optimal L/D forces a pressure distribution nearly symmetric about the root.

Conclusions

A numerical algorithm was developed to ascertain the relevant static aeroelastic characteristics of a flexible micro air vehicle engaged in a rolling maneuver. Roll command is implemented through a torque-rod actuation structure, which forces the wing into an asymmetric wing twist. Numerical procedures involve coupling in-house finite element codes to a vortex-lattice code and show good correlation with experimental data (via wind-tunnel and flight testing). Numerical results indicate a basic tradeoff between wing maneuverability (roll rate) and efficiency (L/D): large wing shaping is needed for roll authority, but leads to a drag penalty. The wing-actuation structure is first optimized for roll rate and L/D by using an enumeration procedure: only single-torque-rod designs are

considered. Theoretical roll rate is improved by 10% over the baseline design used in flight testing, whereas L/D is increased by 6.5%. Next, multiple-torque-rod configurations are considered. A genetic algorithm, in conjunction with a convex combination of the two objective functions, is used to optimize the actuation mechanism with thousands of discrete design permutations. Roll rate and L/D are now improved by 34 and 6%, respectively, over the baseline. Multiple-torque-rod designs typically have smaller displacement fields (compared with single-rod designs) for lower unfavorable twisting moments and drag penalties, whereas the global twisting behavior maintains a large roll rate.

The contributions of this work have significant ramifications in the future design of agile, flexible micro air vehicle wings, particularly with the ever-decreasing size of practical platforms. Controllability concerns may limit the usefulness of wing-shaping designs with maximized maneuverability: MAVs are notoriously difficult to fly. An RC or an autopilot system may not be able to keep pace with a highly maneuverable vehicle. Though a drag metric is not commonly considered in a roll-maneuverability analysis, its inclusion is necessitated by the low Reynolds number nature of the flow over a MAV wing. This becomes particularly true with the demonstrated coupling between efficiency and large wing shaping. Although a key finding of this work is the development of designs with superior maneuverability (compared with a baseline design), perhaps more significant is the identification of methods to maintain the maneuverability of the baseline design without incurring the stringent drag penalty. Formulation of the compromise curve shown earlier allows for selection of an appropriate MAV design based upon the flight specifics: the fidelity of the control system, the experience of the RC pilot, the expected vehicle Reynolds number, etc.

Future work will include expanding the multi-objective optimization scheme, to focus on the torque rod's effect on the aerodynamics of steady level flight. Torque-rod actuation of membrane wings promotes a conflict of interest between the active and the passive shape changes. The presence of a metal torque rod embedded within the membrane wing limits the adaptive washout during steady level flight, making the wing more susceptible to gusts and stall. As in the work described earlier, a multi-objective optimization routine can generate a series of compromise wing designs to detail this tradeoff.

Acknowledgments

This work was supported jointly by the U.S. Air Force Research Laboratory and the U.S. Air Force Office of Scientific Research under F49620-03-1-0381 with Todd Combs, Sharon Heise, and Johnny Evers as project monitors. The authors would also like to acknowledge the technical contributions and funding of Martin Waszak at the NASA Langley Research Center.

References

- [1] Ifju, P., Ettinger, S., Jenkins, D., and Martinez, L., "Composite Materials for Micro Air Vehicles," *SAMPE Journal*, Vol. 37, No. 4, 2001, pp. 7–13.
- [2] Abdulrahim, M., Garcia, H., and Lind, R., "Flight Characteristics of Shaping the Membrane Wing of a Micro Air Vehicle," *Journal of Aircraft*, Vol. 42, No. 1, 2004, pp. 131–137.
- [3] Lazarus, K., Crawley, E., and Bohlmann, J., "Static Aeroelastic Control Using Strain Actuated Adaptive Structures," *Journal of Intelligent Material Systems and Structures*, Vol. 2, No. 3, 1991, pp. 386–410.
- [4] Beauchamp, C., Nadolink, R., Dickinson, S., and Dean, L., "Shape Memory Alloy Adjustable Camber (SMAAC) Control Surfaces," *First European Conference on Smart Structures and Materials*, Proceedings of SPIE—The International Society for Optical Engineering, Vol. 1777, Inst. of Physics Publishing, Bristol, England, U.K., and European Optical Society, Hannover, Germany, 1992, pp. 189–192.
- [5] Albertani, R., Hubner, P., Ifju, P., Lind, R., and Jackowski, J., "Experimental Aerodynamics of Micro Air Vehicles," SAE World Aviation Congress and Exhibition, Reno, NV, Society of Automotive Engineers Paper 2004-01-3090, 2004.
- [6] Fleming, G., and Burner, A., "Deformation Measurements of Smart Aerodynamic Surfaces," 44th Annual SPIE International Symposium on Optical Science, Engineering, and Instrumentation, Denver, CO, International Society for Optical Engineering (SPIE) Paper 3783-25, 1999.
- [7] Albertani, R., Stanford, B., Hubner, P., Lind, R., and Ifju, P., "Experimental Analysis of Deformation for Flexible-Wing Micro Air Vehicles," 2005 AIAA SDM Conference, Austin, TX, AIAA Paper 2005-2231, 2005.
- [8] Lian, Y., Shyy, W., and Ifju, P., "Membrane Wing Model for Micro Air Vehicles," *AIAA Journal*, Vol. 41, No. 12, 2003, pp. 2492–2494.
- [9] Jenkins, C. (ed.), *Gossamer Spacecraft: Membrane and Inflatable Structures Technology for Space Applications*, AIAA Progress in Astrodynamics and Aeronautics Series, Vol. 191, AIAA, Reston, VA, 2001.
- [10] Cook, R., Malkus, D., Plesha, M., and Witt, R., *Concepts and Applications of Finite Element Analysis*, Wiley, New York, 2002.
- [11] Deb, K., *Multi-Objective Optimization Using Evolutionary Algorithms*, Wiley, Chichester, England, U.K., 2001.
- [12] Stanford, B., Albertani, R., and Ifju, P., "Static Finite Element Validation of a Flexible Micro Air Vehicle," *Experimental Mechanics*, Vol. 47, No. 2, 2007, pp. 283–294.
- [13] Drela, M., and Youngren, H., *Athena Vortex Lattice*, Software Package, Ver. 3.15, Massachusetts Inst. of Technology, Cambridge, MA, 2004.
- [14] Goldbach, T., *AVLab—Extended AVL Functionality in MATLAB*, Univ. of Florida, Gainesville, FL, July 2005.
- [15] Khot, N., Eastep, F., and Kolonay, R., "Method for Enhancement of the Rolling Maneuver of a Flexible Wing," *Journal of Aircraft*, Vol. 34, No. 5, 1996, pp. 673–678.
- [16] Haftka, R., and Gurdal, Z., *Elements of Structural Optimization*, Kluwer Academic, Dordrecht, The Netherlands, 1992.
- [17] Chipperfield, A., Fleming, P., Pohlheim, H., and Fonseca, C., "A Genetic Algorithm Toolbox for MATLAB," *Proceedings of the 10th International Conference on Systems Engineering (ICSE '94)*, Coventry Univ., Coventry, England, U.K., 1994, pp. 200–207.